Title: An automated raw tissue precision slicing system for methodological advances in biomedical applications: Streamlining decellularization in porcine cornea-derived tissue-specific bioink fabrication and beyond

Authors: Won Bin Choi[1], Yeon-ju Lee[2], Ju Young Park[2,4], Jinah Jang[1,2,3,4*], Wan Kyun Chung[1]

Affiliations:

[1] Department of Mechanical Engineering, Pohang University of Science and Technology; Pohang, Republic of Korea.

[2] Biobricks Co., Ltd.; Pohang, Republic of Korea.

[3] School of Interdisciplinary Bioscience and Bioengineering, Pohang University of Science and Technology; Pohang, Republic of Korea.

[4] Department of Convergence IT Engineering, Pohang University of Science and Technology; Pohang, Republic of Korea.

*Corresponding author. Email: jinahjang@postech.ac.kr

Preprint of Bio-Design and Manufacturing (unedited)

Abstract:

The decellularized extracellular matrix constitutes a pivotal biomaterial created by decellularizing the natural extracellular matrix (ECM). This material serves as a supportive medium for intricate cellular interactions, fostering cell growth, differentiation, and organization. However, challenges persist in decellularization, necessitating a balance between preserving the structural integrity of the ECM and achieving effective cellular removal. One approach to enhancing decellularization involves pre-eliminating unnecessary tissues, effectively reducing final DNA levels to < 50 ng per mg of ECM on pre-processed tissues. Although this strategic step augments decellularization efficiency, the current manual execution method depends on operator skill. To address this limitation, we propose an automated raw tissue slicing system that does not require prior tissue preparation for slicing. Through carefully controlled tissue applanation pressure and oscillatory incisions with optimized parameters, the system achieved precision < ± 10 μm in obtaining submillimeter tissue slices of the porcine cornea, while

avoiding significant microscopic complications in the tissue structure, as observed by tissue histology. These findings suggest the system's capability to streamline and automate preliminary tissue slicing operations. The efficacy of this approach for decellularization was validated by processing porcine corneas using the proposed system, and subsequently decellularizing the processed tissues. DNA level analysis revealed that sliced, subdivided tissues created by the proposed system could expedite DNA reduction even at the initial steps of the decellularization process, suggesting the promise of enhancing the overall decellularization procedure.

Article Highlights

- Proposed an automated raw tissue slicing system and method with a deviation under 10 µm which requires no tissue preparation for slicing the porcine corneal tissue.
- Examined tissue histology and found no significant complications in the structural integrity of tissues sliced using the suggested system.
- Demonstrated the potential for accelerated DNA reduction in tissues processed by the proposed system.

Preprint of Bio-Design and Manufacturing (unedited)

Keywords: raw tissue slicing, submillimeter slices, high precision, oscillatory incision, applanation, decellularization

1. Introduction

Tissue engineering has made significant advancements in addressing diverse biological and medical challenges. Among its primary areas of focus is the restoration and replacement of damaged tissue, as well as organs. The pivotal components enabling the realization of these objectives are biomaterials, which assume a central role within this field [1]–[4]. The paramount importance lies in the development of microstructures capable of replicating the structural functionalities of the native extracellular matrix (ECM). This capability enables the preservation of the distinctive spatial distribution of both structural and functional components; thus, providing an environment for intricate cellular reactions and assisting cell growth, differentiation, and organization [4]–[9]. A noteworthy biomaterial in this context is the decellularized extracellular matrix (dECM), which is known for its ability to preserve the natural ECM's functional and structural proteins, encompassing various types [10]–[13]. The utilization of dECM in tissue engineering has shown effectiveness across a range of applications, enabling significant restoration of tissue homeostasis and promotion of the regeneration process [1], [10], [21], [11], [14]–[20].

Preprint of Bio-Design and Manufacturing (unedited)

For instance, when a porcine cornea is decellularized, its dECM can be utilized as a key ingredient in various medical applications, particularly in the fabrication of tissue-specific bioinks [21]–[24]. The use of xenogeneic tissues, which are not limited to porcine corneas, offers significant advantages, especially in eliminating the need to find a donor. However, both

allogeneic and xenogeneic tissues, as well as cell-derived ECM, carry risks of interacting with the recipient's body, which could trigger a host-reactive response and potentially cause detrimental effects that hinder in-vivo applications [25], [26]. Such effects include inflammation, foreign-body rejection, and immune reactions, all of which are attributed to the presence of cells or cell-derived materials within the ECM [27]. To mitigate these risks and repopulate new cells, decellularization of tissues and organs is imperative in the manufacturing process of ECM-derived materials [26], [27].

It is difficult to state the status of a target tissue as being decellularized due to the definition is not strictly defined by quantitative metrics. However, various guidelines have been established based on studies in which an *in vivo* constructive remodeling response was observed and adverse cell and host responses were avoided [26], [28], [29]. Two main quantitative criteria are the sample tissue being: 1) < 50 ng dsDNA (double-stranded DNA) per mg dry weight, and 2) < 200 basepair (bp) DNA fragment length [10], [13], [28]–[30].

Diverse decellularization techniques, including enzymatic, chemical, and physical methods, have been developed and refined over time to efficiently remove cellular components from various tissues [10], [26], [31]–[33]. However, a fundamental challenge lies in finding a delicate balance between preserving the structural integrity of the ECM and achieving effective decellularization. Strong decellularization approaches may result in significant ECM disruption or tissue damage [34]–[37]. Meanwhile, methods aimed at preserving the ECM structure and alleviating the influence of the reaction could leave residual cellular debris and may be insufficient on their own to achieve the high degree of cell removal necessary to prevent cell and host responses [10], [21], [38]–[41]. This inherent trade-off highlights the ongoing need for research and innovation to optimize decellularization processes, ensuring that the tissue and

Preprint of Bio-Design and Manufacturing (unedited)

ECM retain their essential properties while becoming suitable for diverse biomedical applications.

To enhance and optimize the decellularization performance, a strategic approach for removing unnecessary tissues can be conducted prior to decellularization [21]. This approach has been applied, for instance, in the case of porcine corneas, where cells were pre-eliminated by manually removing the thin tissue layers from both the top and bottom corneal tissue using a surgical blade, thereby retaining only the stroma. By performing this preliminary tissue removal procedure on a porcine cornea before decellularization, a favorable decellularization outcome can be achieved, resulting in DNA levels < 50 ng/mg. This methodology ensures the attainment of these desired decellularization criteria by eliminating cell layers from the tissue sample. In contrast, the decellularization of porcine corneas without this pre-processing step often results in the decellularization of DNA exceeding the acceptable limit. Notably, the current manual cell removal method requires precise blade control, potentially introducing variability in the quality of pre-decellularization cell removal and prolonging the operation time, making the process highly dependent on the operator's skill level. Therefore, an automated approach for consistent cell removal can eliminate the need for operator involvement.

Automated tissue slicing systems equipped with specially designed blade systems capable of controlling incision parameters have demonstrated the ability to achieve submillimeter-thin tissue slices [42]–[45]. However, their current limitations restrict their application to specific tissue types, such as soft delicate tissues (e.g., brain, liver). Consequently, these systems are not optimized for fibrous organs and connective tissues (e.g., corneal stroma, skin, airway mucosa), which possess robust mechanical properties [42]–[45]. Systems capable of generating thin tissue slices still necessitate the use of tissue-fixation methods (e.g., paraffin wax), adding additional

Preprint of Bio-Design and Manufacturing (unedited)

steps to the overall process. Expanding the range of tissue types that can be sliced by an automated system could facilitate broader application of decellularization process optimization through pre-processing. The current constraints emphasize the necessity for a solution adept at accommodating the distinct mechanical properties exhibited by fibrous organs and connective tissues while ensuring a consistent and effective incision process without the need for prior pre-processing, promoting simplicity and efficiency.

In this study, we developed a coordinated delamination instrument using applanation and cutting (CoDIAC) to validate the use of applanation and oscillatory incision techniques for obtaining precise thin tissue slices of raw porcine cornea tissue. The CoDIAC system employs applanation to securely hold the tissue sample in place and utilizes controlled oscillation to enable precise and effective incisions. By applying carefully controlled pressure to the tissue sample, we achieved uniform flattening and fixation of the tissue. With optimized parameters for oscillatory incisions, we can effectively cut through fibrous tissues without requiring any prior processing, while maintaining uniform submillimeter tissue slices. We verified the slicing performance of CoDIAC by conducting cell pre-elimination slicing experiments on cadaveric porcine eyes, specifically targeting corneal tissue composed of fibrous collagens [46]. In the following stages of our investigation, quantitative analysis was conducted on the processed cornea, followed by tissue histology to meticulously examine the microscopic influence of the system. This investigation yields valuable insights, as the examination of tissue histology allows for inspection of ECM structural integrity and potential microscale complications. The efficacy of the proposed system in the decellularization process was demonstrated by decellularizing corneal tissues processed by CoDIAC. DNA level analysis was performed after each significant

Preprint of Bio-Design and Manufacturing (unedited)

decellularization step, providing data indicating the system's effectiveness in the decellularization process.

The results demonstrate that the core principles employed in corneal tissue slicing by the proposed system effectively enable controlled incisions in fibrous connective tissues of raw porcine corneas. Furthermore, the observed rapid decrease in DNA levels in the processed tissue slices following decellularization suggests potential improvements in efficiency, productivity, and consistency, leading to the potential of streamlining the decellularization process.

2. Method

2.1 Development of a precision tissue slicing system enhanced by applanation and oscillatory incision techniques

The CoDIAC system, an automated tissue slicing tool, was developed to produce thin, submillimeter slices from tissues or organs. It comprises two primary components: an incision module and a vertical stage (Fig. 1). The incision module, equipped with a direct current motor (PGM22-2238-DH, Motor Bank, Seoul, Republic of Korea) linked to a cam mechanism, delivers oscillatory incisions with an adjustable frequency of up to 12 Hz. The frequency of the blade oscillation can be controlled by the input voltage of the motor. Additionally, with the replacement of the cam, the system can further modulate the frequency to four times the base value, offering an additional capability for customized slicing. The current model achieves an oscillation amplitude of up to 15 mm, which can be modified based on the cam size. The vertical stage applies controlled pressure up to 2.8 MPa on the tissue, which is driven by a servo motor (XM430-W210-T, Robotis, Seoul, Republic of Korea) and regulated via a pressure sensor (QA6P, Marvel Dex, Seongnam, Republic of Korea). Each module operates on separate axes, with the incision module moving along the x-axis and the vertical stage along the z-axis (Fig.

Preprint of Bio-Design and Manufacturing (unedited)

1(b)). The incision module length was controlled by a linear actuator (12Lf-10PT-40, IR Robot, Bucheon, Republic of Korea), which offers a maximum speed of 116 mm/s over a 40 mm range and maintains a resolution of 9.75 µm with an accuracy of ± 30 µm or better. CoDIAC ensures automated, consistent tissue slicing under controlled conditions, significantly reducing variability in the slicing process. Table 1 contains comprehensive specifications for the CoDIAC system.

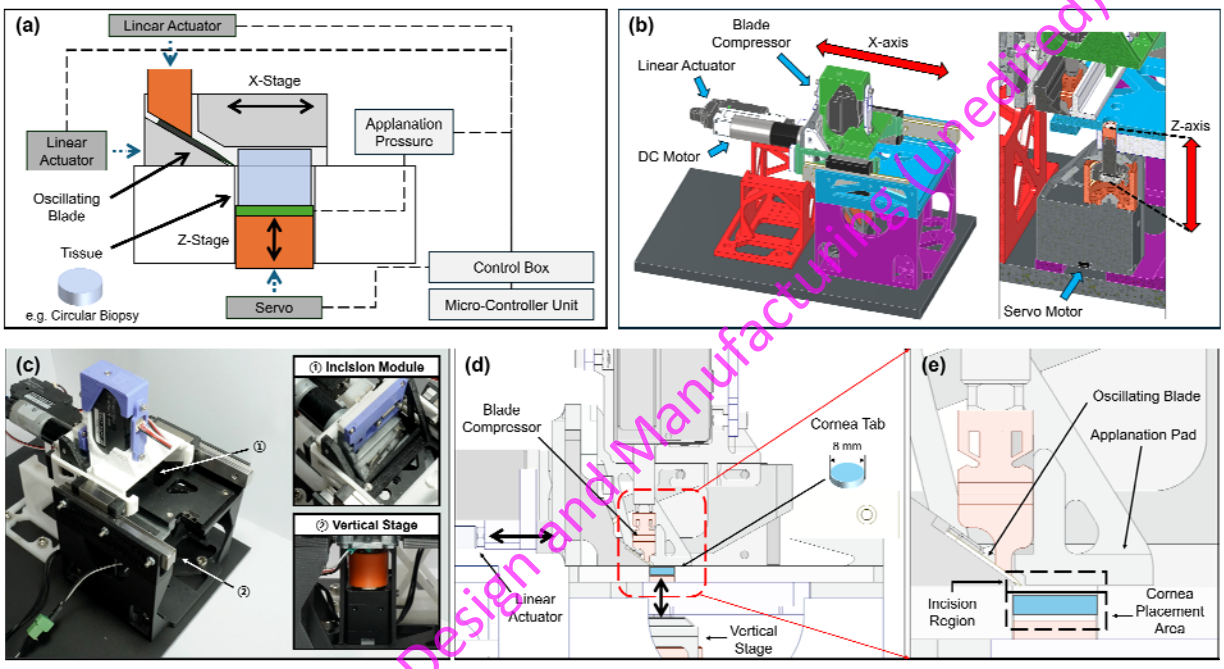

Fig. 1 Structural diagram of the Coordinated Delamination Instrument using Applanation and Cutting (CoDIAC): (a) Functional schematic diagram. (b) 3D CAD model and the internal components. (c) Main function modules of the CoDIAC system. (d) Cross-sectional image of the system mechanism. (e) Close-up view of the applanated incision mechanism.

Preprint of Bio-Design and Manufacturing (unedited)

Table 1 Detailed specifications of the CoDIAC

		Incision Module	Vertical Stage
Drive	Max. Speed	116 mm/s	3.2 mm/s
	Distance	40 mm	14 mm
	Resolution	9.75 µm	0.5 µm
	Accuracy	± 30 µm	± 2.0 µm
	Max. Pressure	-	2.80 MPa
	Motor	Coreless DC Linear Motor	Coreless DC Motor

	Encoder	10 kΩ Linear Potentiometer	Contactless Absolute Encoder
Oscillation	Blade Speed	~ 180 mm/s	-
	Frequency	~ 12 Hz	-
	Amplitude	~ 15 mm	-

Preprint of Bio-Design and Manufacturing (unedited)

2.2 Experiment Design

2.2.1 Shape standardization of the sample tissue

The porcine cornea was pre-processed by extracting the cornea from the central part of a cadaveric porcine eye with an 8 mm biopsy punch. This procedure standardized the target tissue's form into a cylindrical configuration characterized by variable height. Consequently, uniform cylindrical tissue specimens, namely, "cornea tabs", exhibit a consistent diameter but diverse heights. The approximate height of the cornea tab, which represents the central thickness of the porcine cornea, can vary in thickness [47]. Therefore, an adaptive incision method is necessary to accommodate this delicate scale while meeting precise accuracy standards.

2.2.2 Experiment Setup

Cadaver porcine eyes were used for the performance validation of the proposed systems. The porcine eyes were deep-freezed (-80 °C) within 6 hours of enucleation to preserve the samples. Before the experiment, the eyes were thawed by placing them in a 4 °C chiller for 12 hours. Surgical scissors were subsequently used to remove any residual tissues around the eye that had not been removed by the supplier. An 8 mm biopsy punch was utilized to extract a circular tissue sample (referred to as a cornea tab) from the eye. Subsequently, the sample was meticulously rinsed in Phosphate Buffered Saline (PBS) fluid and promptly sliced following a

thorough washing process. The entire procedure of the experiment was recorded for each trial using a DSLR camera (Sony ICLE-7ME) which also included the time data.

2.2.3 Experiment Procedure

During the incision of the given porcine cornea tab, the system goes through four stages of operation: 1) Engagement, 2) Calibration, 3) Incision, and 4) Disengagement. In the engagement phase, the cornea is placed in the cornea placement area and the incision module covers the cornea. The applanation pressure is calibrated once the cornea tab is overlaid with the applanation pad. At this point, the cornea is elevated to the applanation pad in the vertical direction, during which the pressure is gradually increased until the ideal applanation pressure is achieved. Next, the incision begins by operating the oscillating blade and driving the blade at a constant speed. Following complete coverage of the cornea tab area by the blade, the disengagement process involves halting the blade's motion, retracting the oscillating blade, and lowering the processed cornea tab away from the incision region.

Using the proposed device, two distinct tissue slicing methods were applied to porcine cornea tabs. First, consecutive tissue slices were generated through repetitive system operation after the cornea was inserted. This process resulted in multiple slices on the same cornea tab. Second, layer specific tissue sections were created to selectively remove the anterior (epithelium + Bowman's layer) and posterior (endothelium + Descemet's membrane) corneal layers from the cornea tab, separating those layers from the stroma. This involved removing one tissue layer initially and subsequently flipping the cornea tab to address the other tissue layer. The order of anterior and posterior corneal layer removal was randomized.

2.2.4 Measurement and Analysis

Preprint of Bio-Design and Manufacturing (unedited)

To interpret the outcomes of the proposed system, a range of metrics were measured and analyzed, including a post-operative analysis.

1) Thickness: The cornea tab thickness was measured for the entire cornea, consecutive slices, removed anterior and posterior corneal layers, and stroma. Using a micrometer device (Mitutoyo Corporation 293-234-30), the thickness of each sample was acquired with an accuracy of ± 1 µm, a resolution of 1 µm, and an error range of ± 0.3 µm, resulting in a potential reading error of ± 1.7 µm (0.68% margin of error). For precise results, the measurements were taken just prior to tissue deformation by detecting contact between the corneal tissue and the spindle face using a transistor-amplified capacitive touch circuit attached to the spindle faces (Detailed description is provided in the supplementary information). When the spindle face touches the corneal tissue, the light emitting diode will illuminate; therefore, the thickness of the tissue can be measured just before deformation. The complete thickness was measured before the incision, and the thickness of the sliced tissue layers were measured immediately after the incision.

2) Mass: Immediately after the incision, consecutive slices and three tissue layers (stroma, anterior and posterior corneal layers) were measured with an analytical balance (Sartorius BCE224i-1s). The total mass was determined by summing the masses of each individual layer rather than being measured independently. Prior to being placed on the analytical balance, external fluid was removed from all tissue samples by gently tapping them with a non-woven fabric wipe (KM WW-2209) to absorb the fluid.

3) Applanation Pressure: During the incision process, the pressure exerted on the cornea using the vertical stage on the applanation pad was recorded via real-time logging. This record was supplemented with data on applanation pressure, time, and blade drive distance.

Preprint of Bio-Design and Manufacturing (unedited)

Consequently, users can correlate pressure values at specific time points and blade drive distances.

4) Operation Time: Based on the video showing the entire operation of the proposed system, the time required in each step was analyzed for all trials. The start time was set when the cornea tab was positioned onto the designated cornea placement area, while the end time was defined as the moment the cornea was released from the system and lifted clear from the incision site. The operation time in the engagement phase was measured from the start time until the applanation pad fully encompassed the cornea. The calibration phase was recorded until the oscillating blade was activated. Subsequently, the incision phase was tracked until the oscillating blade stopped. The disengagement phase was quantified during the retraction of the blade until the end of the operation.

5) Tissue Histology: Two types of staining were utilized to observe layer removal at the microscopic level. For tissue histology analysis, Hematoxylini and Eosin stain (H&E stain) and 4',6-diamidino-2-phenylindole stain (DAPI stain) were utilized to observe the outcome of the delaminated tissue. The H&E stain enables observation of the overall characteristics of the incision site and assessment of the successful removal of cell layers (epithelium, Bowman's layer, Descemet's layer, and endothelium) by the system. In addition to H&E staining, DAPI staining was concurrently conducted to further examine the presence of DNA. While intralayer cells are present within the stroma, the DAPI-stained tissue histology image helps determine the presence of high-density cell layers on the processed cornea.

6) Decellularized Tissue dsDNA Measurement: After the sample tissues were delaminated using the proposed device, they underwent a decellularization process involving purification (5 mg / 0.2 μL). During the purification task, following each detailed step, portions of the samples

Preprint of Bio-Design and Manufacturing (unedited)

were freeze-dried and subjected to DNA digestion, ensuring accurate quantification of the DNA content in the decellularized samples. DNA quantification utilized the DNA PicoGreen assay, which employs fluorescence intensity for the precise determination of the amount of dsDNA within the samples. For the decellularization task and the dsDNA assays, the GeneJET Genomic DNA Purification Kit (K0722, ThermoFisher Scientific, Massachusetts, United States of America) and the PicoGreen Kit (Quant-iT™ PicoGreen™ dsDNA Assay Kits and dsDNA Reagents), were used respectively.

The solution containing the dECM obtained from the decellularization process underwent dilution, resulting in a dECM concentration of 2.5 mg/mL (C_{dECM}). This concentration served as a correction factor. By utilizing this correction factor, the dsDNA concentration (C_{DNA}) obtained through the PicoGreen assay allows for the determination of the amount of DNA per 1 mg of dECM ($M = C_{DNA}/C_{dECM}$).

Sample tissues processed by the proposed device were categorized into two groups for investigation. In the first group, layer-specific incisions (anterior and posterior corneal layers) were made to obtain the whole stroma. In the second group, consecutive incisions were made on a single piece of corneal tissue, resulting in a subdivided stroma. In both scenarios, the anterior and posterior corneal layers were removed before the decellularization process. To summarize, layer specific incisions yielded a whole cornea, while consecutive incisions resulted in a subdivided stroma. Both were then decellularized, and DNA levels were observed for each group. This systematic comparison aimed to assess the efficacy of the proposed system in the decellularization process.

Preprint of Bio-Design and Manufacturing (unedited)

3. Results and Discussion

3.1 Design and system parameters of the CoDIAC

A microkeratome can offer potential advantages for corneal tissue incisions; however, due to its intended use in short-duration surgical procedures, there are limitations in integrating the microkeratome into the system. Therefore, key incision parameters have been referred to and implemented in the automated system. Slicing is driven by the stress exerted by the blade. This includes shear stress resulting from the blade's motion, where the blade speed is one of the pivotal parameters that influences this shear stress [48]. For stable long-term operation, a low-speed actuator (planetary gear direct current motor – Rated Speed: 398 RPM, Rated Torque: 791 gf-cm) was used instead of a high-speed variant commonly found in microkeratomes. To replicate the oscillation speed of the microkeratome blade with this setup, we lowered the frequency and increased the amplitude of the oscillating blade. The frequency was chosen based on the motor's capability for long-term use and the operation duty cycle. Then, the amplitude was calculated using the following formula: (Oscillation Amplitude) = (Oscillation Frequency) / (Microkeratome Frequency × Microkeratome Amplitude). Therefore, the parameters were

Preprint of Bio-Design and Manufacturing (unedited)

modified to a frequency of 6 Hz and an amplitude of 9.5 mm, yielding a blade speed of 57 mm/s. This adjustment was based on the settings of the Carriazo-Pendular microkeratome's (SCHWIND eye-tech solutions GmbH & Co) instrument settings, which typically exhibit oscillation frequencies ranging from 150-250 Hz [49].

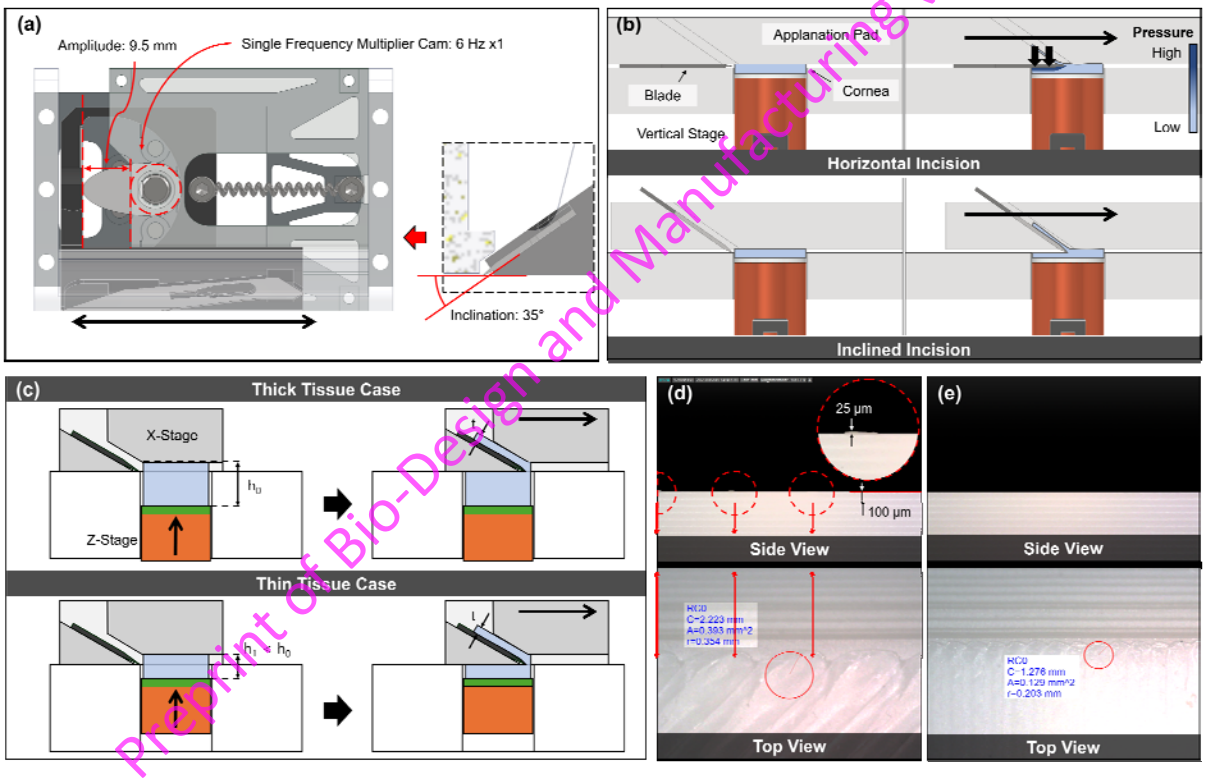

Preprint of Bio-Design and Manufacturing (unedited)

Fig. 2 (a) Incision module design and major parameters. (b) Difference between the horizontal incision and inclined incision. The inclined incision can lessen the effect of blade thickness on corneal tissue samples. (c) An adaptive incision approach to accommodate the variation in tissue thickness. (d) Bumps observed on the applanation pad can potentially lead to complications in the incision performance. (e) Bumps eliminated from the applanation pad after post-processing, ensuring a smooth surface.

The current system was developed to validate the concept of utilizing applanation and oscillatory slicing to achieve effective and precise incisions on raw tissues. Consequently, scalability emerges as another crucial aspect of this research to be further investigated. However, we can contemplate the potential scalability of the system by examining its primary parameters. One of the primary parameters controlled in this system is the blade speed, which remains unaffected by the slice area and is solely influenced by the oscillation frequency and amplitude. While an increased area could indeed influence the applanation pressure, a critical determinant in the slicing outcome of the raw tissue, the vertical stage equipped with a pressure sensor can compensate for such variations. This can be achieved by adjusting the applanation force, effectively compensating for any increase in area. Naturally, if the area is expanded, the vertical stage with the pressure sensor would need to be redesigned to encompass the larger area.

To ensure stable and coordinated oscillatory motion of the blade during tissue incision, we designed an incision module. The module consists of two major design features: 1) a cam mechanism, and 2) an oscillating blade. The cam mechanism linearly oscillates the oscillating blade with a frequency of 6 Hz and a 9.5 mm amplitude which can be driven into the tissue to achieve incision (Fig. 2(a)). However, the thickness of the surgical blade (Feather No. 25 – Thickness: 400 µm) could compress surrounding tissues, generating pressure and shear stress on the tissue plane during incision due to its increased contact area, which might impact the incision performance (Fig. 2(b)). To mitigate this phenomenon, the surgical blade was installed on the oscillating blade at an inclination of 35 degrees relative to the incision plane, in accordance with the angle reference employed in conventional microkeratomes (Fig. 2(c)) [49]. The blade was secured with magnets and a blade compressor to ensure stability.

Preprint of Bio-Design and Manufacturing (unedited)

The height of the cornea tabs can vary depending on the porcine eye sample. Therefore, a passive adaptation method that can accommodate this variation is necessary to achieve a constant incision height. The applanation pad was affixed onto the incision module, ensuring a constant distance between the applanation plane and the oscillating blade's incision plane, keeping the incision height constant regardless of the cornea tab (Supplementary Information Fig. S2). Therefore, the user can control the tissue slice thickness by controlling the distance of the gap between the blade and the applanation pad. The gap distance can be modified by changing the applanation pad installed on the oscillating blade. When the oscillating blade is activated, the cornea tab can be compressed onto the applanation plane and the incision module can slide over the cornea tab, removing a tissue layer of height identical to the specified incision height.

The optimal thickness of the tissue slices may vary depending on the application, and in this study, the thickness was set to 250 µm, which is a large margin to ensure the removal of the cell layers within the corneal tissue. It is important to note that the current system has limitations regarding the usability of slice thickness modification. The slice thickness can be controlled by adjusting the gap distance between the blade and the applanation pad. However, this process requires a removal and installation procedure, which requires the user to follow multiple operation steps. Therefore, introducing a variable gap distance control mechanism integrated into the system could streamline the process of setting the slice thickness, enhancing the usability and efficiency of the system.

The cornea tab was compressed in a coordinated manner by a vertical stage equipped with a pressure measurement function. Compression pressure regulation was achieved using a Proportional Integral Derivative (PID) closed-loop controller. Additionally, the tissue should remain within the designated cornea placement area and incision region to facilitate seamless

Preprint of Bio-Design and Manufacturing (unedited)

operation of the incision module. Therefore, a displacement guard surrounding the vertical stage was installed to inhibit any movement of the cornea tab.

The surface roughness of the applanation pad plays a critical role in ensuring successful incision of the raw tissue. If the pad exhibits surface defects that hinder the achievement of the necessary smoothness, these defects may result in tissue pulling and displacement, potentially leading to incision failure. Moreover, the tissue could be stuck within the incision module due to unexpected tissue relocation. Considering this issue, the applanation pad which was fabricated using fused deposition modeling (FDM) underwent post-processing to ensure a smooth surface and eliminate all surface imperfections (Fig. 2(d), (e)). Smoothness should be achieved, such that when the applanation pad compresses the corneal tissue with a load of 2 kg, the tissue should be able to slide freely with no resistance under the applanation pad.

Preventing contamination when operating and maintaining the device is essential. To facilitate the sterilization process, components that directly contact tissues are designed for easy detachment, utilizing magnetic connections for swift assembly and disassembly from the system. In addition, the blade (Feather No. 25) used in the system is sterile as it undergoes sterilization during the manufacturing process and is sealed in airtight packaging until it is opened for use [50]. After the completion of tissue cutting, the blade can be readily removed and replaced, facilitated by its secure fixation through the use of magnets.

Preprint of Bio-Design and Manufacturing (unedited)

3.2 Submillimeter-scale raw tissue incision and delamination through the CoDIAC

Multiple samples of porcine cornea tissues were used to evaluate the performance of the incisions made by the proposed device. During consecutive incisions, four incisions were made on a single piece of corneal tissue for 10 porcine eyes. For the layer specific case, 10 porcine

eyes were used, and both the anterior and posterior corneal layers were removed from the cornea; thus, two incisions were made on a single sample. To mitigate the potential impacts of the incision sequence, the order of incisions was altered for each trial.

As a result of the consecutive incisions, a single cornea tab was separated into five tissue slices due to the four incisions. The final tissue slice was neglected because it was not sliced in a controlled manner using the proposed system, but rather was a residue of the delamination process. Therefore, using 10 porcine eyes, a total of 40 slices were produced, and the thickness was measured as 252 ± 8 μm. When sliced via a layer specific method, a single porcine cornea sample can be separated into three parts: 1) stroma 2) anterior (epithelium, Bowman's layer) corneal layer 3) posterior (endothelium, Descemet's membrane) corneal layer. The anterior and posterior corneal layers were removed at thicknesses of 252 ± 7 μm (anterior corneal layer) and 251 ± 6 μm (posterior corneal layer), respectively, thereby preserving the stroma at a thickness of 757 ± 48 μm (Fig. 3, Table 2). The target thickness of the sliced tissue using the proposed system was set to 250 μm, and by observation, we could inspect that the sliced tissues followed the target thickness with a variation of 2.4% from the mean (< ± 10 μm).

Given these results, the proposed system can achieve a submillimeter raw tissue incision by utilizing applanation and an oscillating blade. Notably, the target layer removal thickness of 250 μm is large considering the actual thickness of the epithelium, Bowman's layer, Descemet's membrane, and endothelium [47]. However, the target thickness can be modified by changing the applanation pad that is installed on the system (Supplementary Information Fig. S2).

Preprint of Bio-Design and Manufacturing (unedited)

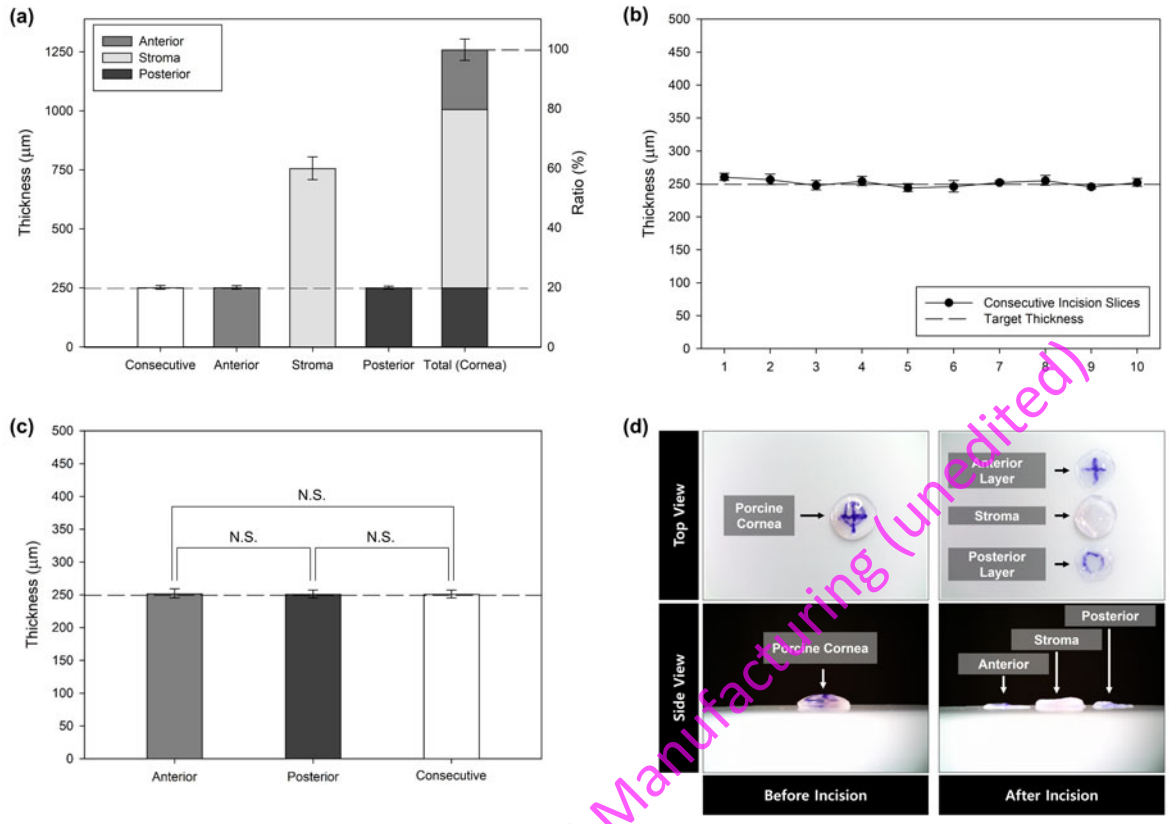

Fig. 3 (a) Slice thickness and ratio of the porcine cornea in consecutive incision (n = 40) case, and layer specific incision case (n = 10) divided into stroma, anterior (epithelium, Bowman's layer) and posterior (endothelium, Descemet's membrane) corneal layers. (b) Layer thickness according to the sample number (order) of the tissue sample by consecutive incision (n = 40). (c) Statistical significance analysis of the sliced layer thickness (n = 10 for each layer, n = 40 for consecutive slices). (d) Porcine cornea sample separated into three parts by raw tissue incision using the proposed device.

Preprint of Bio-Design and Manufacturing (unedited)

Table 2. Thickness of each layer acquired by the system. In the layer specific incision case, the corneal tissue is separated into three layers: stroma, anterior corneal layer (epithelium, Bowman's layer), and posterior corneal layer (endothelium, Descemet's membrane). The black highlights indicate the metrics of the tissue slices.

Unit: μm		Thickness (Target = 250 μm)						
		Consecutive		Layer Specific				
Method	Metrics	Slices	Total (Cornea)	Stroma	Anterior	Posterior	Total (Cornea)	Total (Slices)
CoDIAC	Average	252	1239	757	252	251	1259	251
	STD	8	33	48	7	6	45	6
	Ratio	-	-	60.1 ± 1.0%	20.0 ± 0.9%	20.0 ± 0.9%	-	-
	Error	2	-	-	2	1	-	1
	Size	n = 40	n = 10	n = 10	n = 10	n = 10	n = 10	n = 20

*Error = |Target Thickness – Average Thickness|

Preprint of Bio-Design and Manufacturing (unedited)

3.3 Tissue removal mass measurement and removal precision

The supplementary experiment assessing the slice mass serves as a complementary validation of the slice thickness evaluation conducted previously. From the linear relationship between mass and thickness, congruence is expected between the ratio of thickness/mass measurement of the sliced tissue relative to the total tissue sample. By measuring both the thickness and mass of the tissue slices, we aimed to ensure the accuracy and reliability of our thickness measurements.

Mass measurements were taken of tissues that were mainly composed of extracellular matrix (stroma) and tissues that had high cell density levels (anterior and posterior corneal layers) promptly after the incision. The masses of the removed anterior corneal layer (17.3 ± 0.4 μg) and posterior corneal layer (17.7 ± 0.6 μg) each accounted for 20.6 ± 0.5% and 21.1 ± 0.7%, respectively, of the entire corneal tissue obtained from an 8 mm biopsy punch (Fig. 4, Table 3). The anticipated ratio of the removed mass is expected to exhibit a similar value to that of the thickness, considering the linear relationship between mass and thickness when a constant area is maintained (Table 2, 3).

Given this relationship, the system's ability to create submillimeter-scale thickness incisions with micro-precision directly influences the control of the removed mass. This precision ensures a significant reduction in variability that is often encountered in manual processes. As a result, our system can offer consistently reliable tissue processing that is not dependent on the operator's skill level, which is a critical limitation in manual procedures.

Preprint of Bio-Design and Manufacturing (unedited)

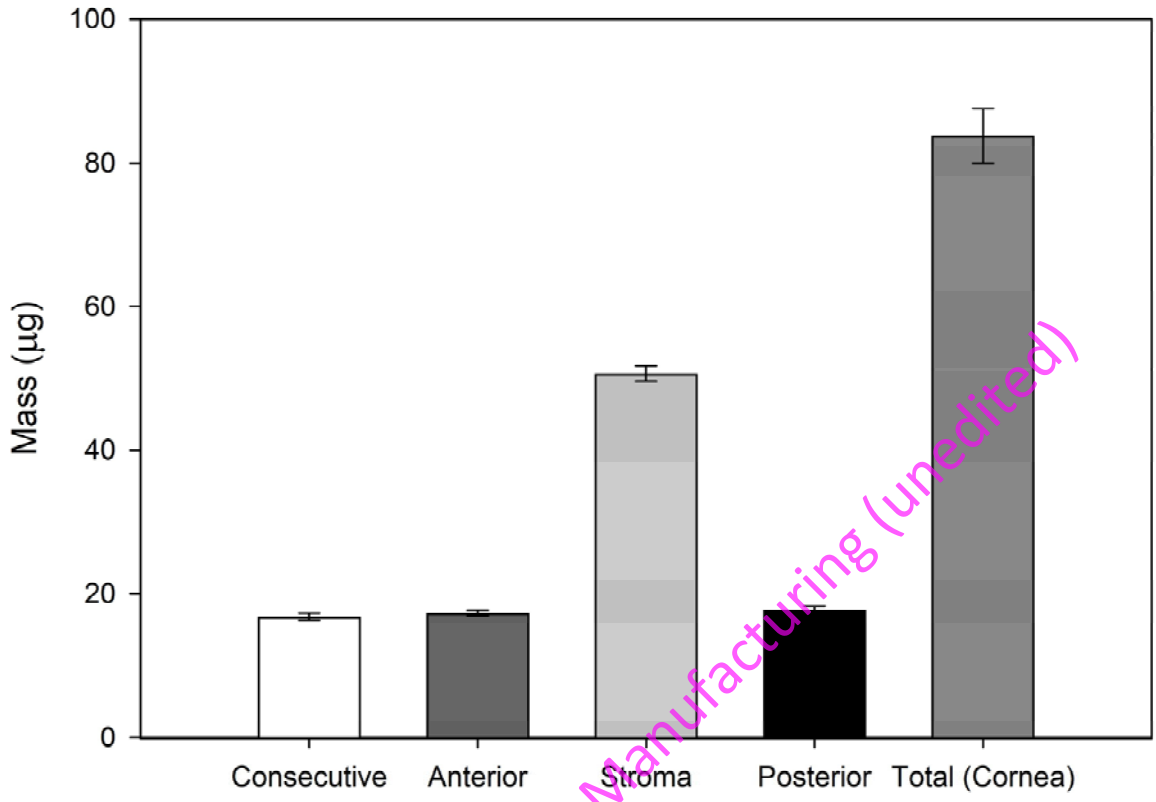

Fig. 4 Acquired mass of the tissue slices in the consecutive incision case (n = 40), and layer specific incision case (n = 10) by the proposed system.

Preprint of Bio-Design and Manufacturing (unedited)

Table 3 Mass of each layer acquired by the system. The black highlights indicate the metrics of the tissue slices.

Unit: µg		Mass						
		Consecutive		Layer Specific				
Method	Metrics	Slices	Total (Slices)	Stroma	Anterior	Posterior	Total (Cornea)	Total (Slices)
CoDIAC	Average	16.8	82.1	50.3	17.3	17.7	83.8	17.5
	STD	0.5	2.5	2.0	0.4	0.6	3.8	0.5
	Ratio			60.0 ± 2.3%	20.6 ± 0.5%	21.1 ± 0.7%	-	-
	Size	n = 40	n = 10	n = 10	n = 10	n = 10	n = 10	n = 20

3.4 Optimal applanation pressure range for effective raw tissue incision and fixation

The optimal applanation pressure for the raw tissue incision of the porcine cornea was 40 ~ 45 kPa. If the pressure drops below the lower limit, premature tearing of the tissue (tissue clipping) may occur, which leaves residual cell layers on the acquired stroma (Fig. 5(b)). Therefore, a Proportional Integral Derivative (PID) controller was utilized to regulate the applanation pressure within the optimal pressure range. The gains of the PID controller were determined using the Ziegler-Nichols method, a heuristic approach for tuning the controller gains [51], [52]. As a result, the clipping phenomenon could be prevented, and a full clean incision of the raw corneal tissue could be created (Fig. 5(c)). Furthermore, it is essential to exercise caution against the application of excessive pressure, as this is crucial for the prevention of potential system failure. This measure also holds significant importance in optimizing the performance of the incision procedure. This is because excessive pressure during tissue applanation can result in heightened friction, potentially generating substantial shear forces on the tissue sample, thus complicating the achievement of an effective incision.

In short, the optimal pressure for fixing the porcine cornea and achieving a submillimeter incision in the raw tissue was found to be within the range of 40 to 45 kPa (Fig. 5). Nonetheless, this pressure was established through a series of iterative experiments conducted on porcine corneal tissue. Therefore, the optimal pressure on different tissue types or organisms might differ. In future research endeavors, an analytic model could be established to predict a suitable pressure range for an arbitrary tissue.

Preprint of Bio-Design and Manufacturing (unedited)

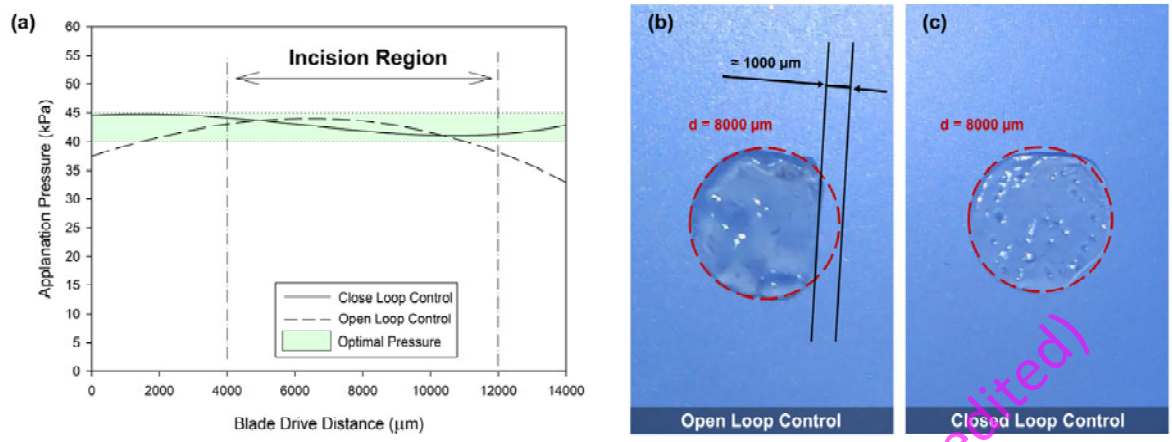

Fig. 5 (a) Applanation pressure on the porcine cornea by blade drive distance during incision. A closed loop proportional integral derivative (PID) controller is required for the regulation of the applanation pressure within the optimal range. (b) Premature tissue tearing (tissue clipping) occurred at the anterior/posterior corneal layer due to an applanation pressure drop -1000 µm ahead of the incision termination point. (c) Tissue clipping was prevented by applying a PID controller for optimal applanation pressure regulation.

Preprint of Bio-Design and Manufacturing (unedited)

3.5 Phase-wise operation time measurement of the CoDIAC

The proposed system goes through four tasks to complete the raw tissue incision of the porcine cornea (Fig. 6). First, during the engagement phase, all the system components are checked, and the sample tissue, which is placed on the vertical stage, is locked into the system (2.00 ± 0.10 sec). Next, in the calibration phase, the vertical stage was controlled to administer the optimal pressure onto the sample tissue (6.30 ± 0.30 sec). After calibration, incision is made (5.62 ± 0.27 sec), and when the blade reaches the end position, the sample tissue is released, and the system is disengaged (3.17 ± 0.15 sec). In summary, the system requires an operation time of 17.09 ± 0.83 sec for the execution of a single layer incision of porcine cornea tissue that is extracted using an 8 mm biopsy punch.

Preprint of Bio-Design and Manufacturing (unedited)

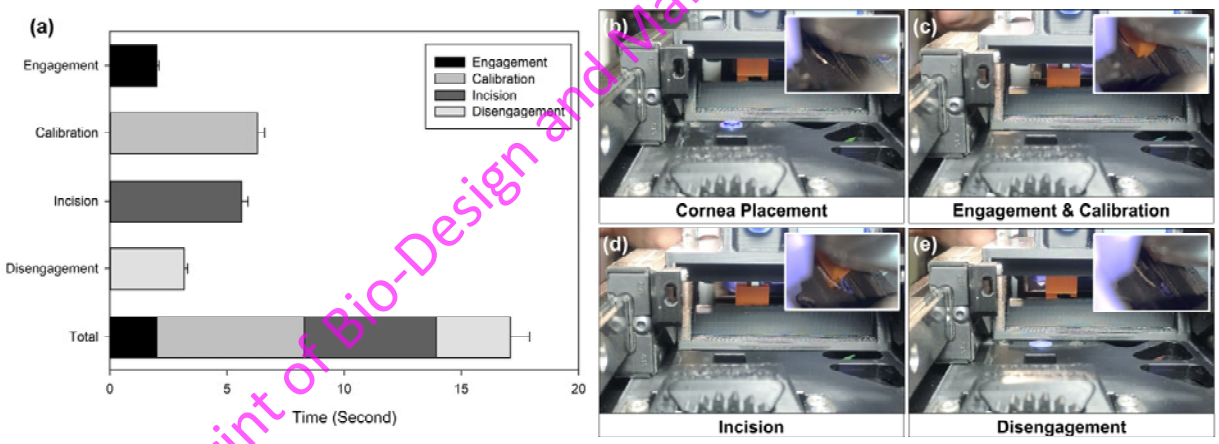

Fig. 6 (a) Operation time of the proposed device by the task type. The cornea layer incision process includes the following steps: (b) Placement of the cornea tab into the cornea placement area – (c) System engagement and calibration of the optimal applanation pressure – (d) Incision made by the oscillating blade – (e) Disengagement of the system, stopping the blade and releasing the cornea tab.

3.6 Cell layer removal efficacy measurement using tissue histology analysis

Although the proposed system demonstrates the ability to effectively delaminate tissue layers, ensuring the complete removal of cell layers requires further microscopic analysis (Fig. 7). Consequently, all samples were examined using cellular staining methods. By inspection of the H&E and DAPI staining images, the porcine cornea control sample is missing the endothelium layer, but the Bowman's layer, Descemet's membrane (DM), and epithelium were intact (Fig. 7(a) – control, (b)). If we observe the tissue sample that has gone under incision by the proposed system, only the stromal membrane is retained and the tissue layers containing the epithelium, Bowman's layer, and DM have been completely removed (Fig. 7(a) – samples, (c)). The removal of the cell layers with high cell density can be inspected by comparing both the H&E and DAPI stain image.

For a better understanding of the system's incision performance, we quantified tissue histology. In the initial step, we assessed the 'score,' representing incision efficacy, through visual inspection and its subsequent rating utilizing a predefined rubric. The evaluation process was based on three specific criteria: 1) 2 points – complete incision and removal of the anterior and posterior corneal layer, 2) 1 point – partial incision and removal of the anterior and posterior corneal layer with some residual regions, 3) 0 point – failure of incision, or if the anterior and posterior corneal layers are intact. In the second step, we assessed the 'cutting rate' by determining whether the cell layers had been removed from the stroma. The evaluation process involved dividing the sample tissue into multiple regions, and a point was assigned if the cell layer was found to be absent.

The cornea sample was divided into three sections (left, middle, right) in both the anterior and posterior regions, resulting in the examination of a total of six sections for each sample (Fig.

Preprint of Bio-Design and Manufacturing (unedited)

7(d)). This structure allowed for a maximum score of twelve points and a maximum cutting rate of six points to be attainable. In summary, the processed tissue samples exhibited an average score of 11.6 (96.7% of the maximum score of 12) and a cutting rate of 5.7 (95% of the maximum of 6) (Table 4, 5). Notably, all the samples demonstrated effective removal of the anterior and posterior corneal layers, apart from complications observed in the fifth and seventh samples (S5, S7).

It is important to mention that in the fifth and seventh samples (S5, S7), at the edge of the cornea tab, the Bowman's layer remained attached to the tab, indicating incomplete removal of the cell layer from the stroma. However, it is worth noting that the corneal thickness in S5 and S7 was greater than that in the other samples. This suggests that the system's ability to achieve stable incisions may be suitable for corneas with a thickness smaller than a certain threshold, beyond which performance might be compromised.

The tissue region where the oscillating blade was used to create the incision had an irregular incision boundary throughout the entire incision area. Although a surgical blade has was in the system, a clean boundary shape could not be obtained. This phenomenon could have been influenced by the blade behavior of having a low oscillation frequency with a high motion amplitude, despite the blade having a similar oscillating speed to that of the microkeratome. Nevertheless, it is worth noting that although the boundary shape could display irregularities, the structural integrity of the stromal tissue remains intact. This observation suggested that the incision method employed by the proposed system results in minimal disturbance to the extracellular matrix architecture and collagen structure. As a result, the risk of potential damage to the basement membrane is likely mitigated.

Preprint of Bio-Design and Manufacturing (unedited)

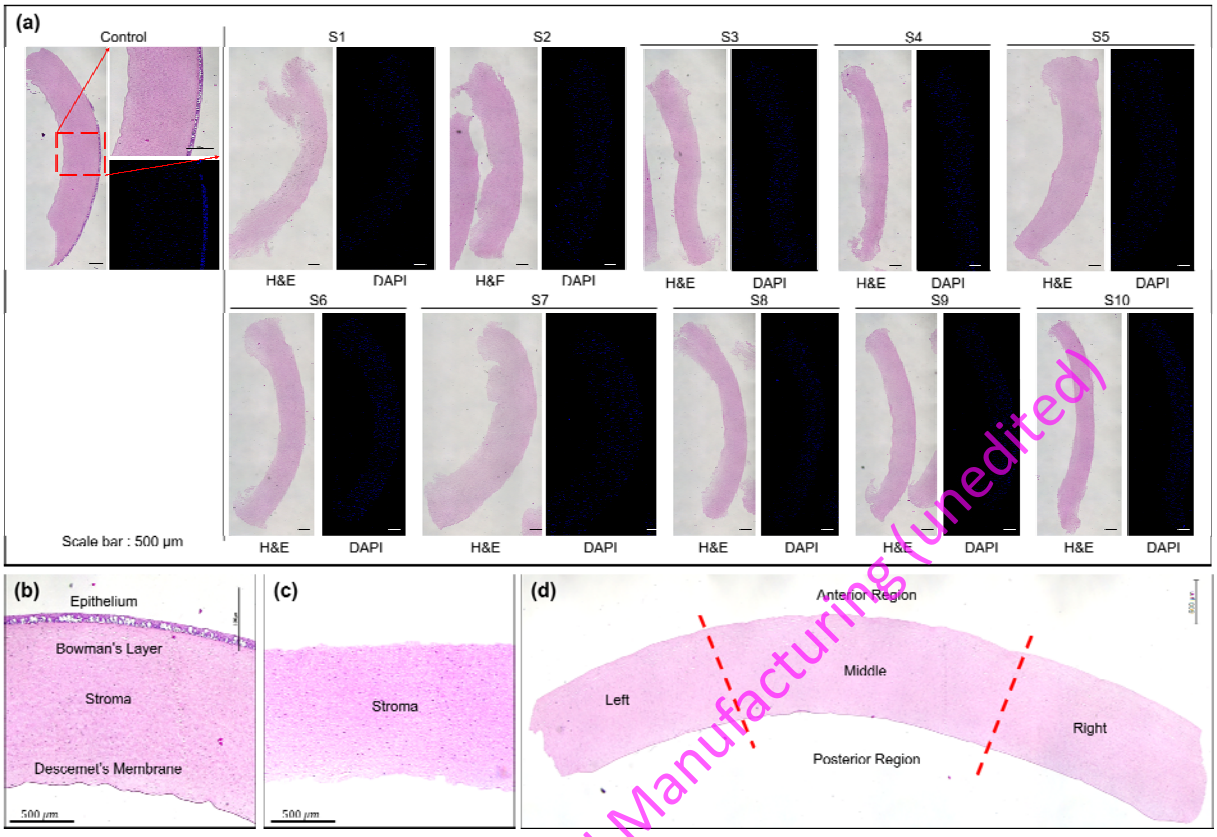

Fig. 7 (a) Tissue histology analysis after slicing the sample tissue by two types of staining: Hematoxylini and Eosin stain (H&E stain) and 4',6-diamidino-2-phenylindole stain (DAPI stain). The histology slides show the state of the sample tissues after the pre-processing state of removing the cell layers before decellularization. It is important to note that nuclear remnants may be partially observed in these slides, as they depict tissues in an intermediate stage of decellularization. A control tissue, involving the extraction of corneal tissue from the porcine eye but without the tissue removal performed by the proposed system, was included for the purpose of comparing the outcomes with those of the processed cornea tabs. The H&E and DAPI staining revealed the staining of cell nuclei, indicating the presence of cells. On inspection, the cell layers (epithelium, Bowman's layer, Descemet's membrane, endothelium) were eliminated when processed using the proposed system. (b) Porcine cornea control sample tissue histology image with H&E stain. (c) Cornea sample that underwent layer removal using the proposed system. By observation, it is possible to inspect that the anterior and posterior corneal tissue layers have been physically removed. (d) Evaluation regions of the processed cornea tissue sample to quantify tissue histology.

Preprint of Bio-Design and Manufacturing (unedited)

Table 4 Performance index value 'score' for tissue histology quantification. Six regions have been inspected and points were assigned based on three quality criteria specified in the evaluation rubric. (Maximum value for each sample: 12 points)

		S1	S2	S3	S4	S5	S6	S7	S8	S9	S10	Average
Anterior Region	Left	2	2	2	2	0	2	2	2	2	2	1.8
	Middle	2	2	2	2	2	2	2	2	2	2	2
	Right	2	2	2	2	2	2	1	2	2	2	1.9
Posterior Region	Left	2	2	2	2	2	2	2	2	2	2	2
	Middle	2	2	2	2	1	2	2	2	2	2	1.9
	Right	2	2	2	2	2	2	2	2	2	2	2
Total		12	12	12	12	9	12	11	12	12	12	11.6
Percentile (%)		100	100	100	100	75.0	100	91.7	100	100	100	96.7

Table 5 Performance index value 'cutting rate' for tissue histology quantification. Six regions have been inspected and points were assigned based on the presence of cell layers. (Maximum value for each sample: 6 points)

	S1	S2	S3	S4	S5	S6	S7	S8	S9	S10	Average
Anterior Region	3	3	3	3	2	3	3	3	3	3	2.9
Posterior Region	3	3	3	3	2	3	2	3	3	3	2.8
Cutting Rate	6	6	6	6	4	6	5	6	6	6	5.7
Percentile (%)	100	100	100	100	66.7	100	83.3	100	100	100	95

Preprint of Bio-Design and Manufacturing (unedited)

3.7 Decellularization efficacy assessment of CoDIAC by DNA level analysis

To investigate the effectiveness of the proposed device, DNA level analysis was conducted on the sample tissues. The analysis involved measuring whole stroma samples (n = 10), where the anterior and posterior corneal layers were removed using the proposed system. Sliced stroma samples (n = 10) were prepared by removing the corneal layers and further slicing the stroma into multiple subdivisions to increase the overall surface area. During the decellularization process, DNA levels were measured after each major step. In comparison to the native stroma (724.90 ± 5.77 ng/mg), the DNA levels of the subdivided sliced stroma (464.19 ± 11.85 ng/mg) showed a significant reduction even at the early steps of the process than those of the whole stroma (702.66 ± 14.41 ng/mg). Beyond achieving lower DNA levels at earlier stages, the sliced subdivided stroma consistently exhibited lower variations in DNA levels ($p < 0.001$, $p < 0.01$) compared to the whole stroma throughout all the measured steps. Additionally, in the sliced stroma case, the DNA level change was insignificant between decellularization steps 1 and 2.

In summary, the results indicate that pre-processing the tissues with the proposed system prior to decellularization can make the sample tissues to achieve a greater degree of reduction in DNA content, as shown in the sliced stroma case. Additionally, the insignificant change observed between the intermediate steps (sliced stroma case – steps 1 and 2) suggests that certain steps (e.g. Decellularization – Step 2) could potentially be omitted, thus simplifying the decellularization process. This optimization has the possibility to reduce the number of required steps, as well as the associated time and financial resources needed for the procedure.

Preprint of Bio-Design and Manufacturing (unedited)

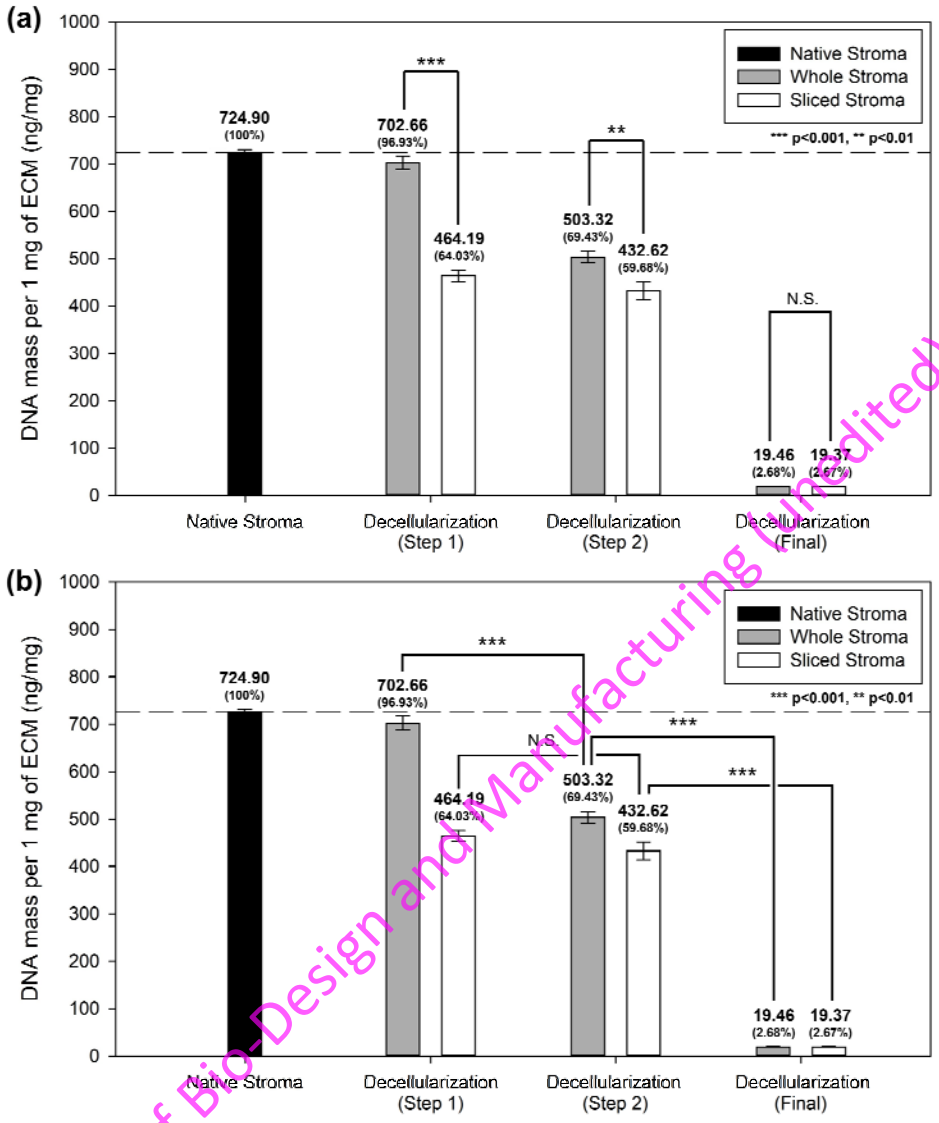

Preprint of Bio-Design and Manufacturing (Unedited)

Fig. 8 DNA levels measured within pre-eliminated cell layer cornea samples that underwent decellularization. Statistical significance analysis was conducted between: (a) sample types and (b) steps for each process. Whole stroma samples (n = 10) were obtained by the layer specific incision method and subdivided sliced stroma samples (n = 10) were obtained by the consecutive incision method. Both the layer specific and consecutive slicing methods involve the removal of the anterior and posterior corneal layers before decellularization, leaving only the stroma. The purification process for decellularization involves several sequential steps. Compared with the whole stroma samples, the sliced stroma samples demonstrated a faster reduction in DNA levels, even during the early steps of the process. Throughout all the steps, the DNA levels in the sliced stroma samples remained consistently lower than those in the whole stroma samples, with significant differences. (*** $p < 0.001$, ** $p < 0.01$)

4. Conclusion

We demonstrated an automated method for achieving high-precision submillimeter raw tissue slicing, eliminating the need for pre-processing. By integrating applanation and an oscillatory incision, we maintained uniform flattening and fixation of the target tissue, generating thin slices with a sliced thickness variability reduced to $< \pm 10$ µm. Confirmed by tissue histology, the system's incision method ensured minimal disturbance to the extracellular matrix architecture and collagen structure, enabling its application in various fields that demand precise submillimeter raw tissue slicing. The stepwise DNA level analysis demonstrated an expedited decrease in DNA levels in the subdivided stroma by the proposed system, even at the initial steps of the decellularization process, which suggests the system's potential to streamline and reduce the necessary steps in the overall decellularization process. The automated high precision submillimeter raw tissue slicing system, CoDIAC, has shown the capability to create precise slices in the fibrous tissues of porcine cornea. Although the fundamental operational principle of raw tissue slicing was demonstrated on the porcine cornea, possible expansion in the application of raw tissue slicing to other organs and tissues can be anticipated. The capabilities demonstrated in this study present a promising opportunity for future research to explore methodological advancements in the field of biomedical research.

Preprint of Bio-Design and Manufacturing (unedited)

Statement and Declarations

- Competing interests: The authors declare that there are no conflict of interest.

- Ethical approval: This study does not contain any studies with human or animal subjects performed by any of the authors.

Acknowledgements: This work was supported by the Alchemist Project 1415180884 (20012378, Development of Meta Soft Organ Module Manufacturing Technology without Immunity Rejection and Module Assembly Robot System) funded By the Ministry of Trade, Industry & Energy (MOTIE, Korea).

This work was supported by the Technology development Program (S3318933) funded by the Ministry of SMEs and Startups (MSS, Korea)

Author contributions: Won Bin Choi designed the study, designed, and fabricated the CoDIAC system, created the control algorithm framework, conducted and analyzed the tissue incision performance. Yeon-ju Lee and Ju Young Park performed the tissue histology and DNA level analysis. Jinah Jang and Wan Kyun Chung supervised the research. All authors revised the final manuscript.

Data availability: The authors confirm that all the data in this manuscript are original and are available from the corresponding author upon reasonable request.

Preprint of Bio-Design and Manufacturing (unedited)

References

[1] J. A. Hubbell, "Biomaterials in tissue engineering," *Bio/Technology*, vol. 13, no. 6, pp. 565–576, 1995, doi: 10.1038/nbt0695-565.

[2] N. Koike, D. Fukumura, O. Gralla, P. Au, J. S. Schechner, and R. K. Jain, "Creation of long-lasting blood vessels," *Nature*, vol. 428, no. 6979, pp. 138–139, 2004, doi: 10.1038/428138a.

[3] M. E. Furth, A. Atala, and M. E. Van Dyke, “Smart biomaterials design for tissue engineering and regenerative medicine,” *Biomaterials*, vol. 28, no. 34, pp. 5068–5073, 2007, doi: 10.1016/j.biomaterials.2007.07.042.

[4] J. H. Collier, J. P. Camp, T. W. Hudson, and C. E. Schmidt, “Synthesis and characterization of polypyrrole-hyaluronic acid composite biomaterials for tissue engineering applications,” *J. Biomed. Mater. Res.*, vol. 50, no. 4, pp. 574–584, Jun. 2000, doi: 10.1002/(SICI)1097-4636(20000615)50:4<574::AID-JBM13>3.0.CO;2-I.

[5] C. E. Schmidt and J. M. Baier, “Acellular vascular tissues: Natural biomaterials for tissue repair and tissue engineering,” *Biomaterials*, vol. 21, no. 22, pp. 2215–2231, 2000, doi: 10.1016/S0142-9612(00)00148-4.

[6] J. Kort-Mascort *et al.*, “Decellularized ECM hydrogels: prior use considerations, applications, and opportunities in tissue engineering and biofabrication,” *Biomater. Sci.*, vol. 11, no. 2, pp. 400–431, 2022, doi: 10.1039/d2bm01273a.

[7] S. M. Busch, Z. Lorenzana, and A. L. Ryan, “Implications for Extracellular Matrix Interactions With Human Lung Basal Stem Cells in Lung Development, Disease, and Airway Modeling,” *Front. Pharmacol.*, vol. 12, May 2021, doi: 10.3389/fphar.2021.645858.

[8] Q. Zhang *et al.*, “Preparation and Application of Decellularized ECM-Based Biological Scaffolds for Articular Cartilage Repair: A Review,” *Front. Bioeng. Biotechnol.*, vol. 10, Jun. 2022, doi: 10.3389/fbioe.2022.908082.

[9] K. Poornima *et al.*, “Implications of Three-Dimensional Cell Culture in Cancer Therapeutic Research,” *Front. Oncol.*, vol. 12, May 2022, doi: 10.3389/fonc.2022.891673.

Preprint of Bio-Design and Manufacturing (unedited)

[10] T. W. Gilbert, T. L. Sellaro, and S. F. Badylak, "Decellularization of tissues and organs," *Biomaterials*, vol. 27, no. 19, pp. 3675–3683, Mar. 2006, doi: 10.1016/j.biomaterials.2006.02.014.

[11] P. J. Schaner *et al.*, "Decellularized vein as a potential scaffold for vascular tissue engineering," *J. Vasc. Surg.*, vol. 40, no. 1, pp. 146–153, Jul. 2004, doi: 10.1016/j.jvs.2004.03.033.

[12] B. N. Brown and S. F. Badylak, "Extracellular matrix as an inductive scaffold for functional tissue reconstruction," *Transl. Res.*, vol. 163, no. 4, pp. 268–285, Apr. 2014, doi: 10.1016/j.trsl.2013.11.003.

[13] E. Garreta *et al.*, "Tissue engineering by decellularization and 3D bioprinting," *Mater. Today*, vol. 20, no. 4, pp. 166–178, 2017, doi: 10.1016/j.mattod.2016.12.005.

[14] B. S. Kim, J. S. Choi, J. D. Kim, Y. C. Choi, and Y. W. Cho, "Recellularization of decellularized human adipose-tissue-derived extracellular matrix sheets with other human cell types," *Cell Tissue Res.*, vol. 348, no. 3, pp. 559–567, Jun. 2012, doi: 10.1007/s00441-012-1391-y.

[15] J. M. Singelyn, J. A. DeQuach, S. B. Seif-Naraghi, R. B. Littlefield, P. J. Schup-Magoffin, and K. L. Christman, "Naturally derived myocardial matrix as an injectable scaffold for cardiac tissue engineering," *Biomaterials*, vol. 30, no. 29, pp. 5409–5416, Oct. 2009, doi: 10.1016/j.biomaterials.2009.06.045.

[16] J. M. Singelyn and K. L. Christman, "Injectable Materials for the Treatment of Myocardial Infarction and Heart Failure: The Promise of Decellularized Matrices," *J.*

Preprint of Bio-Design and Manufacturing (unedited)

Cardiovasc. Transl. Res., vol. 3, no. 5, pp. 478–486, Oct. 2010, doi: 10.1007/s12265-010-9202-x.

[17] D. A. Young, D. O. Ibrahim, D. Hu, and K. L. Christman, "Injectable hydrogel scaffold from decellularized human lipoaspirate," *Acta Biomater.*, vol. 7, no. 3, pp. 1040–1049, Mar. 2011, doi: 10.1016/j.actbio.2010.09.035.

[18] S. B. Seif-Naraghi, D. Horn, P. J. Schup-Magoffin, and K. L. Christman, "Injectable extracellular matrix derived hydrogel provides a platform for enhanced retention and delivery of a heparin-binding growth factor," *Acta Biomater.*, vol. 8, no. 10, pp. 3695–3703, Oct. 2012, doi: 10.1016/j.actbio.2012.06.030.

[19] H. Gudapati, M. Dey, and I. Ozbolat, "A comprehensive review on droplet-based bioprinting: Past, present and future," *Biomaterials*, vol. 102, pp. 20–42, Sep. 2016, doi: 10.1016/j.biomaterials.2016.06.012.

[20] F. Pati, T.-H. Song, G. Rijal, J. Jang, S. W. Kim, and D.-W. Cho, "Ornamenting 3D printed scaffolds with cell-laid extracellular matrix for bone tissue regeneration," *Biomaterials*, vol. 37, pp. 230–241, Jan. 2015, doi: 10.1016/j.biomaterials.2014.10.012.

[21] B. S. Kim, S. Das, J. Jang, and D. W. Cho, "Decellularized Extracellular Matrix-based Bioinks for Engineering Tissue- And Organ-specific Microenvironments," *Chem. Rev.*, vol. 120, no. 19, pp. 10608–10661, Oct. 2020, doi: 10.1021/acs.chemrev.9b00808.

[22] R. Sharifi, Y. Yang, Y. Adibnia, C. H. Dohlman, J. Chodosh, and M. Gonzalez-Andrades, "Finding an Optimal Corneal Xenograft Using Comparative Analysis of Corneal Matrix Proteins Across Species," *Sci. Rep.*, vol. 9, no. 1, p. 1876, Feb. 2019, doi: 10.1038/s41598-018-38342-4.

Preprint of Bio-Design and Manufacturing (unedited)

[23] J. Y. Oh, M. K. Kim, H. J. Lee, J. H. Ko, W. R. Wee, and J. H. Lee, "Processing Porcine Cornea for Biomedical Applications," *Tissue Eng. Part C Methods*, vol. 15, no. 4, pp. 635–645, Dec. 2009, doi: 10.1089/ten.tec.2009.0022.

[24] L. Du, X. Wu, K. Pang, and Y. Yang, "Histological evaluation and biomechanical characterisation of an acellular porcine cornea scaffold," *Br. J. Ophthalmol.*, vol. 95, no. 3, pp. 410–414, Mar. 2011, doi: 10.1136/bjo.2008.142539.

[25] J. M. Aamodt and D. W. Grainger, "Extracellular matrix-based biomaterial scaffolds and the host response," *Biomaterials*, vol. 86, pp. 68–82, Apr. 2016, doi: 10.1016/j.biomaterials.2016.02.003.

[26] P. M. Crapo, T. W. Gilbert, and S. F. Badylak, "An overview of tissue and whole organ decellularization processes," *Biomaterials*, vol. 32, no. 12, pp. 3233–3243, 2011, doi: 10.1016/j.biomaterials.2011.01.057.

[27] S. F. Badylak and T. W. Gilbert, "Immune response to biologic scaffold materials," *Semin. Immunol.*, vol. 20, no. 2, pp. 109–116, Apr. 2008, doi: 10.1016/j.smim.2007.11.003.

[28] S. Nagata, R. Hanayama, and K. Kawane, "Autoimmunity and the Clearance of Dead Cells," *Cell*, vol. 140, no. 5, pp. 619–630, Mar. 2010, doi: 10.1016/j.cell.2010.02.014.

[29] M. H. Zheng, J. Chen, Y. Kirilak, C. Willers, J. Xu, and D. Wood, "Porcine small intestine submucosa (SIS) is not an acellular collagenous matrix and contains porcine DNA: Possible implications in human implantation," *J. Biomed. Mater. Res. Part B Appl. Biomater.*, vol. 73B, no. 1, pp. 61–67, Apr. 2005, doi: 10.1002/jbm.b.30170.

Preprint of Bio-Design and Manufacturing (unedited)

[30] S. Das, G. Gao, J. Y. Lee, J. Jang, and D.-W. Cho, “Decellularized Tissue Matrix-based 3D Tissue Modeling,” in *Biofabrication and 3D Tissue Modeling*, The Royal Society of Chemistry, 2019, pp. 148–170. doi: 10.1039/9781788012683-00148.

[31] J. E. Arenas-Herrera, I. K. Ko, A. Atala, and J. J. Yoo, “Decellularization for whole organ bioengineering,” *Biomed. Mater.*, vol. 8, no. 1, p. 014106, Jan. 2013, doi: 10.1088/1748-6041/8/1/014106.

[32] T. Hoshiba, H. Lu, N. Kawazoe, and G. Chen, “Decellularized matrices for tissue engineering,” *Expert Opin. Biol. Ther.*, vol. 10, no. 12, pp. 1717–1728, Dec. 2010, doi: 10.1517/14712598.2010.534079.

[33] T. J. Keane, I. T. Swinehart, and S. F. Badylak, “Methods of tissue decellularization used for preparation of biologic scaffolds and in vivo relevance,” *Methods*, vol. 84, pp. 25–34, Aug. 2015, doi: 10.1016/j.ymeth.2015.03.005.

[34] A.-M. Kajbafzadeh, N. Javan-Farazmand, M. Monajemzadeh, and A. Baghayee, “Determining the Optimal Decellularization and Sterilization Protocol for Preparing a Tissue Scaffold of a Human-Sized Liver Tissue,” *Tissue Eng. Part C Methods*, vol. 19, no. 8, pp. 642–651, Aug. 2013, doi: 10.1089/ten.tec.2012.0334.

[35] J. Zhou *et al.*, “Impact of heart valve decellularization on 3-D ultrastructure, immunogenicity and thrombogenicity,” *Biomaterials*, vol. 31, no. 9, pp. 2549–2554, Mar. 2010, doi: 10.1016/j.biomaterials.2009.11.088.

[36] W.-C. Jiang, Y.-H. Cheng, M.-H. Yen, Y. Chang, V. W. Yang, and O. K. Lee, “Cryo-chemical decellularization of the whole liver for mesenchymal stem cells-based functional

Preprint of Bio-Design and Manufacturing (unedited)

hepatic tissue engineering," *Biomaterials*, vol. 35, no. 11, pp. 3607–3617, Apr. 2014, doi: 10.1016/j.biomaterials.2014.01.024.

[37] P. F. Gratzer, R. D. Harrison, and T. Woods, "Matrix Alteration and Not Residual Sodium Dodecyl Sulfate Cytotoxicity Affects the Cellular Repopulation of a Decellularized Matrix," *Tissue Eng.*, vol. 12, no. 10, pp. 2975–2983, Oct. 2006, doi: 10.1089/ten.2006.12.2975.

[38] D. E. Heath, "A Review of Decellularized Extracellular Matrix Biomaterials for Regenerative Engineering Applications," *Regen. Eng. Transl. Med.*, vol. 5, no. 2, pp. 155–166, Jun. 2019, doi: 10.1007/s40883-018-0080-0.

[39] F. Kabirian and M. Mozafari, "Decellularized ECM-derived bioinks: Prospects for the future," *Methods*, vol. 171, pp. 108–118, Jan. 2020, doi: 10.1016/j.ymeth.2019.04.019.

[40] S.-H. Hung, C.-H. Su, F.-P. Lee, and H. Tseng, "Larynx Decellularization: Combining Freeze-Drying and Sonication as an Effective Method," *J. Voice*, vol. 27, no. 3, pp. 289–294, May 2013, doi: 10.1016/j.jvoice.2013.01.018.

[41] M. Ahearne and A. Coyle, "Application of UVA-riboflavin crosslinking to enhance the mechanical properties of extracellular matrix derived hydrogels," *J. Mech. Behav. Biomed. Mater.*, vol. 54, pp. 259–267, Feb. 2016, doi: 10.1016/j.jmbbm.2015.09.035.

[42] C. L. Krumdieck, J. dos Santos, and K.-J. Ho, "A new instrument for the rapid preparation of tissue slices," *Anal. Biochem.*, vol. 104, no. 1, pp. 118–123, May 1980, doi: 10.1016/0003-2697(80)90284-5.

Preprint of Bio-Design and Manufacturing (unedited)

[43] D. Majorova *et al.*, "Use of Precision-Cut Tissue Slices as a Translational Model to Study Host-Pathogen Interaction," *Front. Vet. Sci.*, vol. 8, Jun. 2021, doi: 10.3389/fvets.2021.686088.

[44] P. F. Smith *et al.*, "Dynamic organ culture of precision liver slices for toxicology," *Life Sci.*, vol. 36, no. 14, pp. 1367–1375, Apr. 1985, doi: 10.1016/0024-3205(85)90042-6.

[45] *An Atlas of Comparative Vertebrate Histology*. Elsevier, 2018. doi: 10.1016/C2012-0-06909-8.

[46] L. L. S. N. J. V. H. S. W. P. K. A. Alm, *Adler's Physiology of the Eye*. Elsevier Inc., 2011.

[47] M. Crespo-Moral, L. García-Posadas, A. López-García, and Y. Diebold, "Histological and immunohistochemical characterization of the porcine ocular surface," *PLoS One*, vol. 15, no. 1, 2020, doi: 10.1371/journal.pone.0227732.

[48] E. Shamoto and Y. Altıntas, "Prediction of Shear Angle in Oblique Cutting with Maximum Shear Stress and Minimum Energy Principles," *J. Manuf. Sci. Eng.*, vol. 121, no. 3, pp. 399–407, Aug. 1999, doi: 10.1115/1.2832695.

[49] A. Behrens, A. Langenbucher, M. M. Kus, C. Rummelt, and B. Seitz, "Experimental evaluation of two current-generation automated microkeratomes: The Hansatome and the Supratome," *Am. J. Ophthalmol.*, vol. 129, no. 1, pp. 59–67, 2000, doi: 10.1016/S0002-9394(99)00269-X.

[50] FEATHER Safety Razor Co., "Surgery - Surgical Blade & Handle Catalog." https://www.feather.co.jp/en/pdf/m_Products/surgery2112.pdf (accessed Sep. 13, 2023).

[51] J. G. Ziegler and N. B. Nichols, "Optimum Settings for Automatic Controllers," *J. Fluids Eng.*, vol. 64, no. 8, pp. 759–765, Nov. 1942, doi: 10.1115/1.4019264.

Preprint of Bio-Design and Manufacturing (unedited)

[52] A. S. McCormack and K. R. Godfrey, “Rule-based autotuning based on frequency domain identification,” *IEEE Trans. Control Syst. Technol.*, vol. 6, no. 1, pp. 43–61, 1998, doi: 10.1109/87.654876.

Preprint of Bio-Design and Manufacturing (unedited)